Huang et al. Nanoscale Research Letters (2016) 11:249
DOI 10.1186/s11671-016-1461-2

Nanoscale Research Letters

NANO EXPRESS Open Access

Gold Nanoparticles of Diameter 13 nm Induce Apoptosis in Rabbit Articular Chondrocytes

Hao Huang[1], Ying-yao Quan[1], Xiao-ping Wang[1*] and Tong-sheng Chen[2]

Abstract

Gold nanoparticles (AuNPs) have been widely used in biomedical science including antiarthritic agents, drug loading, and photothermal therapy. In this report, we studied the effects of AuNPs with diameters of 3, 13, and 45 nm, respectively, on rabbit articular chondrocytes. AuNPs were capped with citrate and their diameter and zeta potential were measured by dynamic light scattering (DLS). Cell viability was evaluated by Cell Counting Kit-8 (CCK-8) assay after the rabbit articular chondrocytes were pre-incubated with 3, 13, and 45 nm AuNPs, respectively, for 24 h. Flow cytometry (FCM) analysis with annexin V/propidium iodide (PI) double staining and fluorescence imaging with Hoechst 33258 staining were used to determine the fashion of AuNPs-induced chondrocyte death. Further, 13 nm AuNPs (2 nM) significantly induced chondrocyte death accompanying apoptotic characteristics including mitochondrial damage, externalization of phosphatidylserine and nuclear concentration. However, 3 nm AuNPs (2 nM) and 45 nm (0.02 nM) AuNPs did not induce cytotoxicity in chondrocytes. Although 13 nm AuNPs (2 nM) increased the intracellular reactive oxygen species (ROS) level, pretreatment with Nacetyl cysteine (NAC), a ROS scavenger, did not prevent the cytotoxicity induced by 13 nm AuNPs, indicating that 13 nm AuNPs (2 nM) induced ROS-independent apoptosis in chondrocytes. These results demonstrate the size-dependent cytotoxicity of AuNPs in chondrocytes, which must be seriously considered when using AuNPs for treatment of osteoarthritis (OA).

Keywords: Gold nanoparticles, Chondrocyte apoptosis, Size-dependent cytotoxicity, Osteoarthritis

Background

Osteoarthritis (OA) is the most common and disability joint disease [1, 2]. Treatments of OA are divided into non-surgical interventions for patients in early and moderate stages and surgery interventions for patients in advanced stages according to the severity of OA [3–5]. OA therapy was mainly to reduce pain and increase life quality of the OA patient [6]. Oral non-steroidal anti-inflammatory drugs (NSAIDs), the most efficacious and widely used treatments for knee OA, have shown some risks of systemic adverse events including gastrointestinal or cardiovascular abnormalities [7]. In this light, local treatments appear to be preferable especially in older OA patients with comorbidities [7]. Although intra-articular injection of hyaluronic acid may be a viable alternative to NSAIDs for knee OA [7], its clinical use is still controversial [8]. Because of the inefficacy and "not cost-effective" of intra-articular injection of hyaluronic acid, three clinical practice guidelines, including the National Institute for Health and Care Excellence (UK), National Collaborating Centre for Chronic Conditions (UK), and American Academy of Orthopaedic Surgeons (USA), were recommended against the use of intra-articular injection of hyaluronic acid in the treatment of knee OA [8]. In addition, multiple intra-articular injections of hyaluronic acid, which may increase the risk of joint infection, are needed due to the short residence time of hyaluronic acid in joint [9, 10]. It was also reported that intra-articular injection of corticosteroids might increase adverse effects including joint infection, intra-articular and periarticular calcifications, cutaneous atrophy and cutaneous depigmentation when

* Correspondence: txp2938@jnu.edu.cn
[1]Department of Pain Management, The First Affiliated Hospital of Jinan University, Guangzhou 510630, China
Full list of author information is available at the end of the article

used repeatedly for OA treatment [11]. Therefore, it is currently desired to develop a new clinical methodology for OA treatment.

Gold colloid or gold salts can exert anti-inflammation effect by downregulating the expression of interleukin-1β, prostaglandin E2, and cyclooxygenase-2 [12–15], which plays a crucial role in the pathogenesis of OA [16–21]. Recently, it was reported that mice model of OA, after treatment with gold nanoparticles (AuNPs) combined with curcumin, presented less severe in the histological lesions [22]. Similarly, AuNPs (7–130 nm) capped with different drugs exhibited potential treatment for OA [23–25]. Our recent studies demonstrated that reactive oxygen species (ROS) played a key role in chondrocyte apoptosis that had been reported to be correlated with the severity of OA [26, 27]. AuNPs (~3.5 and ~50 nm) have been demonstrated to be a potential antioxidant [28, 29]. ~64.83 nm AuNPs capped with hyaluronate and tocilizumab showed therapeutic effects on rats with collagen-induced arthritis (CIA) [30]. Similarly, 13 nm AuNPs capped with galectin-1 showed therapeutic effects on CIA rats [31], and 13 nm AuNPs capped with citrate could also ameliorate CIA in rats [15, 32].

Toxicity of AuNPs (1.4–65 nm), an inevitable issue for its biomedical applications, is related to its size, surface group, dose, and incubation time as well as cell line [33–35]. It is worth noting that 50 nm AuNPs are harmful for human OA chondrocytes [36], while 5 nm AuNPs capped with porcine type II collagen enhance chondrocytes growth in 10-kg Yorkshire pigs [37]. This report aims to study the size-dependent cytotoxicity of AuNPs in rabbit articular chondrocytes. It was reported that 18 nm AuNPs (0–500 pM) capped with citrate induced dose-dependent cytotoxicity in Hela cells [38], and we selected similar concentration (0–2 nM) to study the cytotoxicity of AuNPs in our system. The AuNPs size of our preparation is 3, 13, and 45 nm, respectively, just covering the size of 1–100 nm (Fig. 1a), and AuNPs with this size range seem to have more practical significance [15, 24, 30–32]. Our data demonstrates that 13 nm AuNPs capped with citrate induce chondrocyte apoptosis, whereas 3 and 45 nm AuNPs are nontoxic in chondrocytes.

Methods

Reagents

2′, 7′-Dichlorofluorescin diacetate (DCFH-DA), Nacetyl cysteine (NAC), Rhodamine 123 (Rho 123), Hoechst 33258 and $HAuCl_4$ were from Sigma (St. Louis, MO, USA). Dulbecco's Modified Eagle's Medium (DMEM) was from Gibco (Carlsbad, CA, USA), fetal bovine serum (FBS) was from Sijiqing (Hangzhou, Zhejiang, China). Cell Counting Kit-8 (CCK-8) was from Dojindo (Kumamoto, Japan). Annexin V-FITC/propidium iodide (PI) apoptosis detection kit was from Bender Medsystems (Vienna, Austria). Mitotracker Deep Red 633, Trypsin and type II collagenase were from Invitrogen (Carlsbad, CA, USA). Sodium citrate dehydrate was purchased from Sinopharm Group Chemical Regent Co., Ltd. (Shanghai, China).

Preparation of AuNPs

As described previously, 13 nm AuNPs were prepared by the citrate reduction of $HAuCl_4$ [39]. All glass wares were cleaned in aqua regia (3 parts HCl, 1 part HNO_3) and rinsed with MilliQ water. A solution of $HAuCl_4$ (1 mM, final concentration) in MilliQ water (50 mL) in a three-necked flask with a condenser and a thermometer was heated while stirring. After boiling had commenced, trisodium citrate solution (5 mL, 38.8 mM) was added quickly, which resulted in a change in solution color from pale yellow to deep red. After the color change, the solution was kept stirring for additional 15 min and then slowly cooled down to room temperature.

It is possible to control the size of AuNPs from 5 to 150 nm by simply varying the reaction conditions [40–43]. We prepared 3 nm AuNPs by changing the ratio of sodium citrate to gold salt. Similar to the preparation of 13 nm AuNPs, aqueous solution of $HAuCl_4$ (50 mL, 0.29 mM) was brought to a three-necked flask with a condenser and a thermometer while stirring and boiling, and trisodium citrate solution (4 mL, 34 mM) was added quickly after boiling had commenced, which resulted in a change in solution color from pale yellow to deep red. After the color change, we stopped boiling and kept stirring for additional 15 min to cool it to room temperature.

Although working very hard, we failed to prepare AuNPs more than 13 nm in diameter. Finally, we purchased 45 nm AuNPs from British BioCell International (BBI, Cardiff, UK, 60 nm AuNPs named by BBI), and the concentration of these particles was ~0.04 nM according to spectrophotometry measurement. Therefore, the highest concentration of 45 nm AuNPs was 0.02 nM in our system, while the highest concentration was 2 nM for both 3 and 13 nm AuNPs.

The formation of AuNPs was analyzed with a UV-vis spectrophotometer (Lambda 35, Perkin-Elmer, USA). The diameter and zeta potential of AuNPs were measured by dynamic light scattering (DLS, $n = 3$, Zetasizer Nano, Malvern Instrument Co., UK).

Cell Isolation and Culture

Articular chondrocytes for primary culture were harvested from slices of shoulder, knee and hip-joint cartilage from

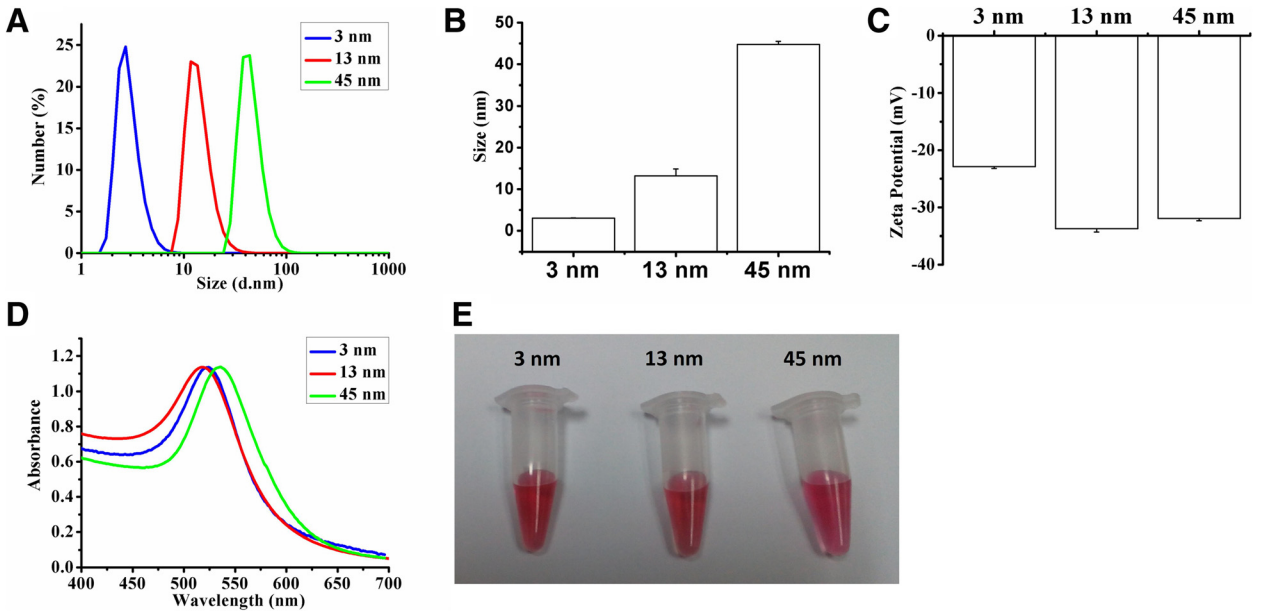

Fig. 1 Characterization of AuNPs. **a** The size distribution of 3, 13, and 45 nm AuNPs by number. **b**, **c** The hydrodynamic diameters and zeta potentials of 3, 13, and 45 nm AuNPs ($n = 3$). **d** Photographic images and UV-vis spectra of 3, 13, and 45 nm AuNPs. **e** Color of 3, 13, and 45 nm AuNP solutions

4-week-old New Zealand white rabbits under aseptic conditions as described previously [26]. The cartilage was separated from the subchondral bone and cut into small pieces (2–3 mm^2) using a sterile surgical blade, and chondrocytes from the small pieces were then isolated by enzymatic digestion of 0.25 % Trypsin in PBS for 1 h and 0.2 % type II collagenase in DMEM for 4–6 h at 37 °C in humidified atmosphere containing 5 % CO_2. After collection by centrifugation (4 °C, 3000 RPM, 5 min), chondrocytes were resuspended in DMEM supplemented with 10 % FBS and antibiotics (100 U/ml penicillin and 100 U/ml streptomycin), and then seeded in culture flasks at 37 °C in humidified 5 % CO_2 as monolayer culture. The primary cells were sub-cultured to generation 2 that were cultured in DMEM supplemented with 10 % FBS and antibiotics for at least 24 h.

The second generation of chondrocytes was used for all experiments, and the cell confluence should reach approximately 80 % of the area of culture flask before experiments. Chondrocytes were treated with AuNPs for 8 h for the assay of cytochrome c release, mitochondrial morphology, and apoptosis, and for 24 h for other's experiments without special indication.

Characterization of Cell Death

Cell viability was detected by CCK-8 assay according to the manufacturer's instructions as described previously [44, 45]. Cells were plated in 96-well plates (1.3×10^4 cells/well) for 24 h at 37 °C and then subjected to the indicated treatments, including treatment with 3 nm AuNPs (0–2 nM), 13 nm AuNPs (0–2 nM) and 45 nm AuNPs (0–0.02 nM), respectively, for 24 h, and treatment with 13 nm AuNPs (2 nM) for 0, 3, 6, 12 and 24 h, respectively. Afterward, 90 μl DMEM and 10 μl CCK-8 solutions were added to each sample, and after incubation at 37 °C in humidified 5 % CO_2 for 30 min, the optical density of each sample was measured at 450 nm using an auto-microplate reader (Infinite M200, Tecan, Austria). Four parallel replicates were read for each sample.

Apoptosis rate was measured by flow cytometry (FCM) analysis using annexin V/PI apoptosis detection kit as described previously [26]. After treatment with AuNPs for 8 h, the cells were washed with PBS, suspended by trypsinization, harvested by centrifugation (4 °C, 3000 RPM, 5 min) and resuspended in 400 μl binding buffer at a concentration of 9×10^5 cells/ml, and then 5 μl annexin V was added into binding buffer and incubated for 15 min in dark (4 °C). Afterward, 10 μl PI was added into the above solution for 5 min in dark (4 °C) before a further addition of 600 μl PBS. Apoptosis rate was assessed by FCM analysis with annexin V/PI apoptosis detection kit, and 10,000 events were recorded for each FCM analysis.

Apoptotic morphological changes in the nuclear chromatin of cells were detected by Hoechst 33258 staining. Chondrocytes were seeded on a confocal dish. After treatment with AuNPs for 24 h, the cells were fixed with 4 % paraformaldehyde for 10 min and washed with PBS, followed by incubation with Hoechst 33258 staining

(10 μM, final concentration) for 30 min in dark (37 °C). After three washes with PBS, chondrocytes stained with Hoechst 33258 were imaged by a fluorescence microscope (Axiovert 200 M, Zeiss).

Measurement of Intracellular ROS

Intracellular ROS levels were measured with DCFH-DA as described previously [46, 47]. Chondrocytes cultured in 6-wells plates for 24 h were subjected to the indicated treatments. DCFH-DA (20 μM, final concentration) was added to different groups of chondrocytes and the cells were then incubated in a dark and humidified atmosphere (5 % CO_2, 37 °C) for 30 min. Afterward, the cells were washed with PBS, suspended by trypsinization, harvested by centrifugation (4 °C, 3000 RPM, 5 min), resuspended in 1 ml PBS and finally analyzed by FCM with 488 nm excitation and 525 nm emission detection. Values of cellular fluorescence were obtained using FCS Express Version 3.

In addition, we studied whether ROS played a key role for the cytotoxicity induced by 13 nm AuNPs. NAC, a potent antioxidant, can prevent chondrocyte death by scavenging ROS [26, 27]. NAC was prepared just before the experiments by dissolving the powders in MilliQ water. Chondrocytes plated in 96-well plates for 24 h were pre-incubated with NAC (2 mM, final concentration) for 2 h, and then co-treated with 13 nm AuNPs (2 nM) and H_2O_2 (0.5 mM, final concentration), respectively, for 24 h before CCK-8 assay.

Measurement of Mitochondrial Membrane Potential (ΔΨm)

Rho 123 was used to analyze ΔΨm by FCM as described previously [26, 46]. Cells were stained with Rho 123 (6 μM, final concentration) for 30 mins at 37 °C in dark, and then washed with PBS, suspended by trypsinization, harvested by centrifugation (4 °C, 3000 RPM, 5 min), resuspended in 1 ml PBS and subsequently assayed by FCM with 488 nm excitation and 515 nm emission. Values of cellular fluorescence were obtained using FCS Express Version 3.

The ΔΨm in single living cells was also monitored in real-time by time-lapse confocal imaging as described previously [46]. Briefly, the fluorescence images of cells stained with 6 μM Rho 123 were monitored in real-time using a confocal microscope (LSM510/ConfoCor2, Zeiss, Jena, Germany) equipped with a device sustained culture condition (37 °C, 5 % CO_2) .

Detection of Cytochrome c Release

Chondrocytes were transiently transfected with green fluorescent protein-cytochrome c (GFP-Cyt.c, provided by Dr. G. J. Gores) [48]. Thirty-six hours after transfection, the cells were treated with 13 nm AuNPs for 8 h, washed with PBS and imaged by the fluorescence microscope (IX73, Olympus, Japan). The GFP-Cyt.c released from mitochondria was determined based on the GFP-Cyt.c fluorescence images. GFP was excited at 488 nm and its fluorescence emission was recorded through a 500–530 nm IR band-pass filter.

Observation of Mitochondrial Morphology

Cells were cultured on a confocal dish. After treatment with 3, 13, and 45 nm AuNPs for 8 h, the cells were washed with PBS and incubated with Mitotracker Deep Red 633 (0.1 μM, final concentration) for 30 min at room temperature in dark. The cells were then washed with PBS and visualized under confocal microscope (LSM510/ConfoCor2, Zeiss, Jena, Germany). Mitotracker Deep Red 633 was excited at 633 nm, and the emitted light was recorded through a 650-nm long-pass filter.

Statistical Analysis

Data were presented as mean ± SD from three independent experiments, and all of experiments repeated three times. Data were analyzed by student's t test using SPSS 17.0. P values less than 0.05 were considered to be statistically significant.

Results

Characterization of AuNPs

The hydrodynamic size and surface charge of AuNPs were analyzed by DLS (Fig. 1a–c). Fig. 1a shows a representative DLS analysis on the size distribution of AuNPs, and the hydrodynamic size of three diameters of AuNPs was ca. 2.94 nm (indicated as 3 nm in our text), ca. 13.19 nm (indicated as 13 nm in our text) and ca. 44.74 nm (indicated as 45 nm in our text), respectively (Fig. 1b). The corresponding zeta potential was −22.9 ± 0.3 mV for 3 nm AuNPs, −33.76 ± 0.58 mV for 13 nm AuNPs and −31.93 ± 0.41 mV for 45 nm AuNPs (Fig. 1c). The surface plasmon resonance peak of 3, 13, and 45 nm AuNPs appeared around 523, 520, and 535 nm, respectively (Fig. 1d). All of the 3, 13, and 45 nm AuNPs solutions remained red in color (Fig. 1e), a characteristic of AuNPs particles less than 100 nm in diameter [49].

13 nm AuNPs Induce Cytotoxicity in Rabbit Articular Chondrocytes

CCK-8 assay showed that treatment with 13 nm AuNPs (0.02, 0.2 and 2 nM) for 24 h induced dose-dependent cytotoxicity, while treatment with 3 nm AuNPs (0.002, 0.02, 0.2, and 2 nM) or 45 nm AuNPs (0.002 and 0.02 nM) for 24 h did not induce cytotoxicity (Fig. 2a). Moreover, 13 nm AuNPs (2 nM) induced a potent time-dependent cytotoxicity (Fig. 2b). Microscopic images showed that 13 nm AuNPs (2 nM) significantly induced chondrocyte death, while 3 nm AuNPs (2 nM) and

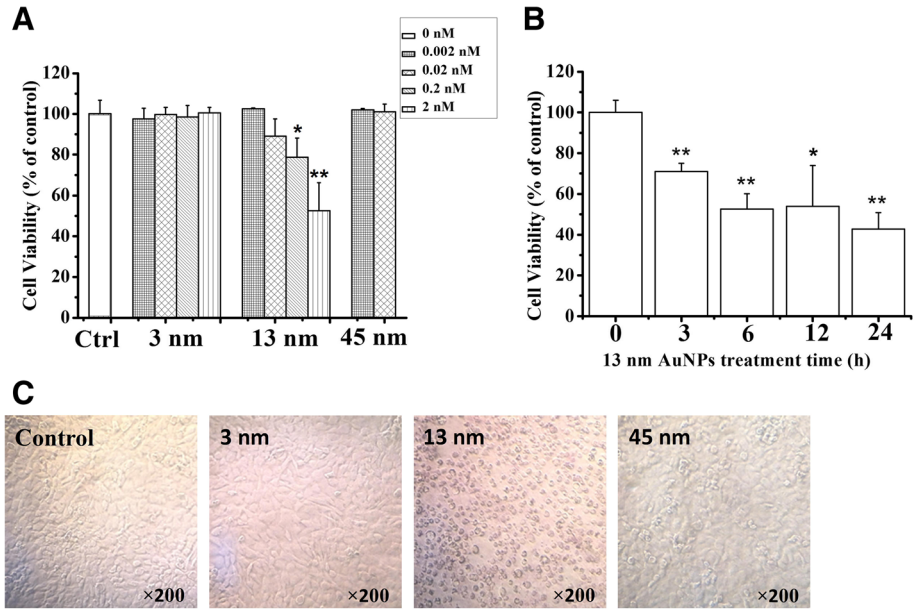

Fig. 2 AuNPs induce cytotoxicity in rabbit articular chondrocytes. **a** cytotoxicity of 3, 13, and 45 nm AuNPs. *$P < 0.05$ and **$P < 0.01$, compared with control. **b** time-dependent cytotoxicity of 13 nm AuNPs. *$P < 0.05$ and **$P < 0.01$, compared with control. **c** Microscopic images of chondrocytes after treatment with 3, 13, and 45 nm AuNPs, respectively, for 24 h. Original magnification: ×200

45 nm AuNPs (0.02 nM) did not induce chondrocyte death (Fig. 2c).

13 nm AuNPs Induce Apoptosis in Rabbit Articular Chondrocytes

We next used FCM analysis with annexin V/PI staining to determine whether 13 nm AuNPs induced apoptosis in chondrocytes. Annexin V was used to detect phosphatidylserine externalization which was a hallmark of the early apoptosis, and PI was used to label DNA fragments, a symbol of cell death. Q3 area (both annexin V and PI are negative) represents the intact and healthy cells. Q4 (annexin V is positive and PI is negative) represents the early apoptotic cells and Q2 (both annexin V and PI are positive) represents the late apoptosis. As shown in Fig. 3a, 86.37 % cells were gathered together at Q3 area in the control group, and the percentages of apoptotic cells (Q2 + Q4) in the control, 3 and 45 nm AuNPs groups were less than 12 %. However, after treatment with 13 nm AuNPs (2 nM) for 8 h, the percentage of apoptotic cells (Q2 + Q4) increased to 46.61 %, demonstrating that 13 nm AuNPs induced chondrocyte death in apoptotic fashion, which was further verified by the fluorescence images of chondrocytes stained with Hoechst 33258 (Fig. 3c).

13 nm AuNPs Induce Apoptosis via Mitochondrial Damage

FCM analysis with Rho 123 staining showed that 13 nm AuNPs induced a significant decrease of ΔΨm, while 3 and 45 nm AuNPs did not induce a decrease of ΔΨm (Fig. 4a, b). Dynamical loss of ΔΨm in single living cells stained with potential-sensitive dye Rho 123 was also monitored by imaging the reduction of Rho 123 fluorescence using a time-lapse confocal microscope. The time-lapse images of cells stained with Rho 123 are shown in Fig. 4c. We found that compared with control cells, 13 nm AuNPs treatment induced a significant decrease of Rho 123 fluorescence, further confirming the notion that 13 nm AuNPs induce chondrocyte apoptosis via mitochondrial damage.

We next monitored cytochrome c release from mitochondria in single living cells using the fluorescence microscope. As shown in Fig. 4d, in contrast to control cells, the cells treated with 13 nm AuNPs exhibited an even distribution of the GFP-Cyt.c in the entire cytoplasm, indicating that 13 nm AuNPs induced the release of cytochrome c from mitochondria. We also assessed the effect of AuNPs on the mitochondrial morphology by using confocal fluorescence microscope, and found that in contrast to the normal long tubular mitochondria in control cells, the mitochondria of the cells treated with 13 nm AuNPs became punctate and swollen (Fig. 4e), further demonstrating the notion that 13 nm AuNPs induced damage of mitochondria.

13 nm AuNPs Induce Cytotoxicity Independent of ROS

Finally, we examined whether ROS was involved in the cytotoxicity of 13 nm AuNPs. We firstly used FCM assay with DCFH-DA to evaluate AuNPs-induced ROS

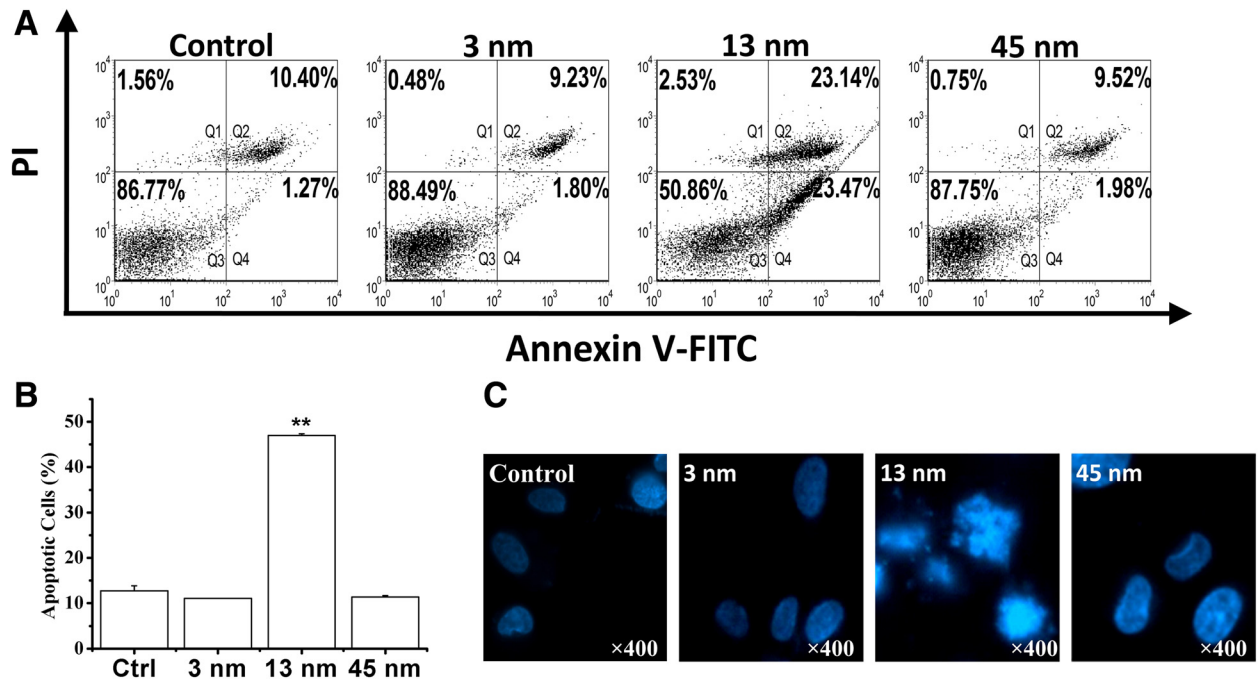

Fig. 3 13 nm AuNPs induce apoptosis in rabbit articular chondrocytes. **a** FCM analysis with annexin V/PI staining on chondrocytes apoptosis induced by 3, 13, and 45 nm AuNPs, respectively. **b** Statistical results from three independent FCM analyses. $^{**}P < 0.01$, compared with control. **c** Fluorescence imaging of chondrocytes stained with Hoechst 33258 after treatment with 3, 13, and 45 nm AuNPs, respectively, for 24 h. Original magnification: ×400

production, and found that treatment with three diameters of AuNPs for 24 h induced a significant ROS generation (Fig. 5a, b). CCK-8 assay showed that NAC pretreatment prevented 500 μM H_2O_2-induced cell death but did not prevent 13 nm AuNPs-induced cytotoxicity (Fig. 5c), demonstrating that 13 nm AuNPs induced cytotoxicity possibly independent of ROS.

Discussion

Our results support the notion that AuNPs induce size- and dose-dependent cytotoxicity in chondrocytes. Furthermore, this report for the first time demonstrates that 13 nm AuNPs capped with citrate induce chondrocyte apoptosis by the mitochondrial pathway. Although AuNPs induce ROS generation, the ROS may be not involved in the cytotoxicity of AuNPs.

Our findings that 13 nm AuNPs induce chondrocyte apoptosis but 3 and 45 nm AuNPs are nontoxic (Figs. 2a and 3) demonstrate the size-dependent toxicity of AuNPs in chondrocytes. We noted that 1.2 nm AuNPs capped with triphenylphosphine monosulfonate (TPPMS) rather than 15-nm particles induced apoptosis in Hela cells [35], whereas larger AuNPs (25 nm), when capping with polyvinyl pyrrolidone, caused more cytotoxicity in Hela cells compared to smaller particles (2 and 10 nm) [34]. Similarly, in vivo studies in mice also showed different size-dependent toxicity of AuNPs capped with different surface groups (citrate or polyethylene glycol) [50, 51]. The different size-dependent toxicity in the same cell line or animal may be related to the different surface groups of AuNPs. Although 13 nm AuNPs capped with citrate caused cytotoxicity in rabbit articular chondrocytes (Fig. 2), 10 nm AuNPs were reported to be nontoxic in dendritic cells [52]. In addition, 33 nm AuNPs capped with citrate were found to be non-cytotoxic to baby hamster kidney cells and human hepatocellular liver carcinoma cells, but cytotoxic to a human carcinoma lung cell line [53]. Therefore, the size-dependent cytotoxicity of AuNPs is also related to cell line.

Many drugs that are beneficial at low doses are toxic at high doses [33]. Similarly, 1.2 or 1.4 nm AuNPs at high doses showed dose-dependent cytotoxicity in vitro study [35, 54]. Further, 13 nm AuNPs at low dose (0.2–2 nM) showed dose-dependent cytotoxicity in rabbit articular chondrocytes (Fig. 2a). It was reported that 50 nm AuNPs less than 80 μM were found to be non-cytotoxic, while 160 μM of 50 nm AuNPs was harmful for human OA chondrocytes [36]. Consequently, we conclude that 13 nm AuNPs are more toxic than 50 nm AuNPs in chondrocytes.

Our data demonstrate that 13 nm AuNPs induce cell death by mitochondrial damage (Fig. 4), which is

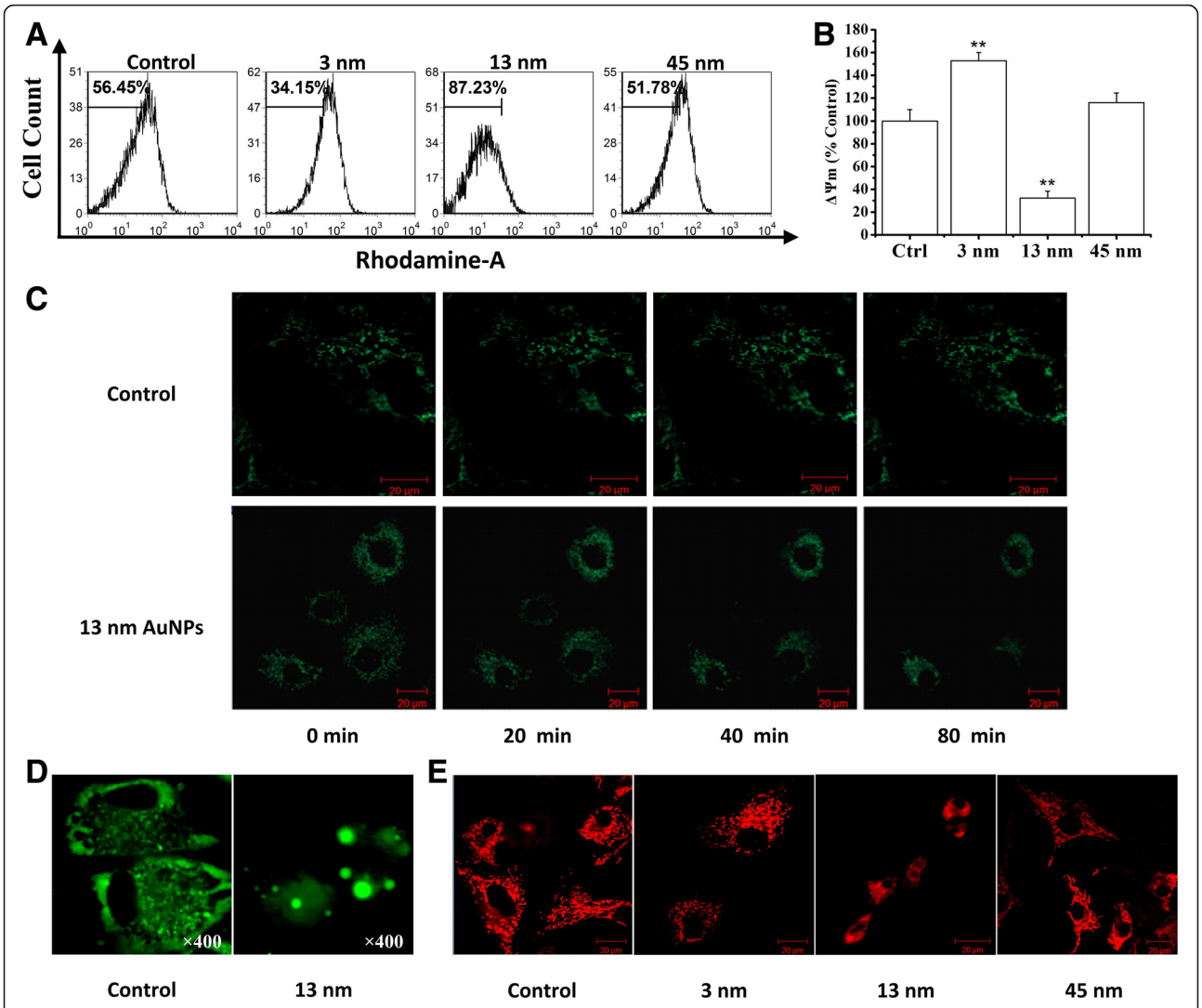

Fig. 4 13 nm AuNPs induce apoptosis by mitochondrial damage. **a** FCM analysis with Rho 123 staining on the loss of ΔΨm induced by 3, 13, and 45 nm AuNPs, respectively. **b** Statistical results from three independent FCM analyses. $^{**}P < 0.01$, compared with control. **c** Time-lapse imaging of cells stained with Rho 123 after treatment with 13 nm AuNPs for 8 h. *Scale bar* 20 μm. **d** Fluorescence imaging of chondrocytes transfected with GFP-Cyt.c after treatment with 13 nm AuNPs for 8 h. Original magnification: ×400. **e** Confocal imaging of chondrocytes stained with Mitotracker Red 633 after treatment with 3, 13, and 45 nm AuNPs, respectively, for 8 h. *Scale bar* 20 μm

consistent with Pan and coworkers' report [54]. Similarly, in contrast to 2 and 10 nm AuNPs, it was reported that 25 nm AuNPs aggregated in the mitochondria of HeLa cells and caused cytotoxicity [34]. Recently, Mkandawire and coworkers' reported that 20 nm AuNPs targeted into mitochondria of breast cancer cells, caused partial rupture of the outer mitochondrial membrane and finally induced apoptosis [55]. These findings proved that mitochondrial damage induced by AuNPs played a crucial role in cell death. Interestingly, 3 nm AuNPs significantly enhanced the proportion of cells with high mitochondrial membrane potential (Fig. 4a, b). Dwivedi and coworkers found that 13 nm AuNPs combined with chondroitin sulfate induced the growth of chondrocytes and also enhanced the production of extracellular matrix components [24]. These data suggest that AuNPs with specific size have the potential ability to trigger chondrocyte growth.

Formation and degradation of the extracellular matrix are important for cartilage. Extracellular matrixes, including collagens, proteoglycans, and noncollagenous proteins, play a key role in forming a macromolecular framework to stabilize tissue [56]. Compared to chondrocytes grown in monolayer culture (two-dimensional structure), animal experiments (three-dimensional structure) may be more suitable for the study of extracellular

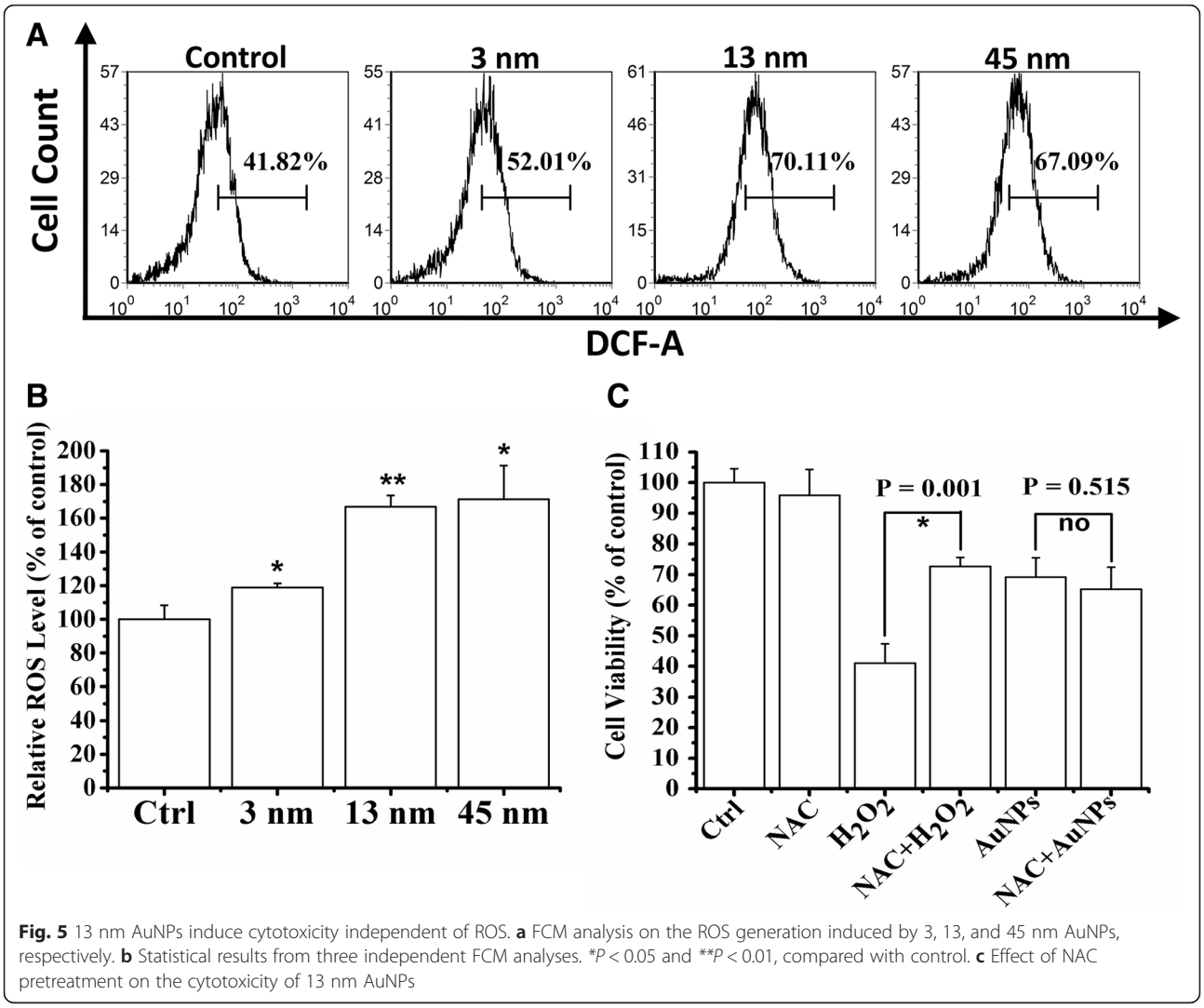

Fig. 5 13 nm AuNPs induce cytotoxicity independent of ROS. **a** FCM analysis on the ROS generation induced by 3, 13, and 45 nm AuNPs, respectively. **b** Statistical results from three independent FCM analyses. *$P < 0.05$ and **$P < 0.01$, compared with control. **c** Effect of NAC pretreatment on the cytotoxicity of 13 nm AuNPs

matrix. Therefore, we are going to evaluate the effect of AuNPs on the extracellular matrix formation and degradation in mice OA model in the near future.

Although 13 nm AuNPs increased ROS product in chondrocytes (Fig. 5a, b), the fact that NAC pretreatment did not prevent its cytotoxicity (Fig. 5c) suggests that 13 nm AuNPs induce ROS-independent cytotoxicity. Similarly, Tay and coworkers found that ~2 nm Au nanoclusters capped with mercaptopropionic acid increased ROS product in both mitochondria and cytoplasm, but it did not lead to any detrimental cellular effects in human derived colonic epithelial NCM460 cells [57]. In fact, the effect of AuNPs on ROS production is still controversial. Inhibiting ROS production was considered as a remarkable property of AuNPs [29, 49]. Hsieh and coworkers found that compared to epigallocatechin-3-gallate (EGCG), ~50 nm EGCG-AuNPs conjugates had stronger ability to scavenge ROS [28]. Similar result was also reported by another study on the articular chondrocytes of 10-kg Yorkshire pigs [37]. However, there was publication reported that AuNPs could significantly induce surface group-dependent intracellular ROS generation [58]. It was reported that 1.4 nm AuNPs capped with TPPMS triggered necrosis by oxidative stress in Hela cells [54]. Therefore, the role of ROS in AuNPs-induced cytotoxicity may depend on cell lines and the surface groups of AuNPs.

Although 3 and 13 nm AuNPs were prepared by the same method, the two particles had different zeta potential values (Fig. 1c), further demonstrating the notion that the zeta potential value of nanoparticles is associated with the size of the particles. It was reported that zeta potential values were related to particles' electrophoretic mobility [59]. In addition, previous studies indicated that the electrophoretic mobility of colloidal particles (in the same medium) was related to the size of particles, and that the electrophoresis mobility increased with the increasing radius of colloid particles, which might be due to the relaxation effect of smaller particles [60].

Conclusions

While 3 and 45 nm AuNPs are nontoxic, 13 nm AuNPs induce cytotoxicity in rabbit articular chondrocytes. Moreover, 13 nm AuNPs induce chondrocyte apoptosis via mitochondrial damage independent of ROS. Our findings further remind those who use AuNPs for treatment of OA should pay attention to the size-dependent cytotoxicity of AuNPs in chondrocytes.

Abbreviations

AuNPs: gold nanoparticles; CCK-8: Cell Counting Kit-8; CIA: collagen-induced arthritis; DCFH-DA: 2′, 7′-dichlorofluorescin diacetate; DLS: dynamic light scattering; DMEM: Dulbecco's Modified Eagle's Medium; EGCG: epigallocatechin-3-gallate; FBS: fetal bovine serum; FCM: flow cytometry; GFP-Cyt.c: green fluorescent protein-cytochrome c; NAC: nacetyl cysteine; NSAIDs: non-steroidal anti-inflammatory drugs; OA: osteoarthritis; PI: propidium iodide; Rho 123: rhodamine 123; ROS: reactive oxygen species; TPPMS: triphenylphosphine monosulfonate; ΔΨm: mitochondrial membrane potential.

Competing Interests

The authors declare that they have no competing interests.

Authors' Contributions

HH and TC conceived and designed the experimental strategy. HH and YQ performed the experiments and prepared the manuscript. TC and XW supervised the whole work and revised the manuscript. All authors read and approved the final manuscript.

Acknowledgements

This work was supported by the National Natural Science Foundation of China (grants 61527825, 81572184 and 81471699) and the Natural Science Foundation of Guangdong (grant 2014A030313378). We thank Dr. G. J. Gores for providing the GFP-Cyt.c plasmid.

Author details

[1]Department of Pain Management, The First Affiliated Hospital of Jinan University, Guangzhou 510630, China. [2]MOE Key Laboratory of Laser Life Science and College of Biophotonics, South China Normal University, Guangzhou 510006, China.

Received: 26 November 2015 Accepted: 3 May 2016
Published online: 13 May 2016

References

1. Ma Z, Piao T, Wang Y, Liu J (2015) Astragalin inhibits IL-1beta-induced inflammatory mediators production in human osteoarthritis chondrocyte by inhibiting NF-kappaB and MAPK activation. Int Immunopharmacol 25:83–87
2. van der Kraan PM, van den Berg WB (2012) Chondrocyte hypertrophy and osteoarthritis: role in initiation and progression of cartilage degeneration? Osteoarthr Cartilage 20:223–232
3. Dieppe PA, Lohmander LS (2005) Pathogenesis and management of pain in osteoarthritis. Lancet 365:965–973
4. Mero A, Campisi M, Favero M, Barbera C, Secchieri C, Dayer JM, Goldring MB, Goldring SR, Pasut G (2014) A hyaluronic acid-salmon calcitonin conjugate for the local treatment of osteoarthritis: chondro-protective effect in a rabbit model of early OA. J Control Release 187:30–38
5. Noth U, Steinert AF, Tuan RS (2008) Technology insight: adult mesenchymal stem cells for osteoarthritis therapy. Nat Clin Pract Rheu 4:371–380
6. Koszowska A, Hawranek R, Nowak J (2014) Osteoarthritis—a multifactorial issue. Rheumatology 5:319–325
7. Bannuru RR, Vaysbrot EE, Sullivan MC, McAlindon TE (2014) Relative efficacy of hyaluronic acid in comparison with NSAIDs for knee osteoarthritis: a systematic review and meta-analysis. Semin Arthritis Rheum 43:593–599
8. Altman RD, Schemitsch E, Bedi A (2015) Assessment of clinical practice guideline methodology for the treatment of knee osteoarthritis with intra-articular hyaluronic acid. Semin Arthritis Rheum 45:132–139
9. Altman RD, Akermark C, Beaulieu AD, Schnitzer T, Durolane International Study G (2004) Efficacy and safety of a single intra-articular injection of non-animal stabilized hyaluronic acid (NASHA) in patients with osteoarthritis of the knee. Osteoarthr Cartilage 12:642–649
10. Di Sante L, Cacchio A, Scettri P, Paoloni M, Ioppolo F, Santilli V (2011) Ultrasound-guided procedure for the treatment of trapeziometacarpal osteoarthritis. Clin Rheumatol 30:1195–1200
11. Leighton R, Akermark C, Therrien R, Richardson JB, Andersson M, Todman MG, Arden NK, Group DS (2014) NASHA hyaluronic acid vs. methylprednisolone for knee osteoarthritis: a prospective, multi-centre, randomized, non-inferiority trial. Osteoarthr Cartilage 22:17–25
12. Nieminen R, Korhonen R, Moilanen T, Clark AR, Moilanen E (2010) Aurothiomalate inhibits cyclooxygenase 2, matrix metalloproteinase 3, and interleukin-6 expression in chondrocytes by increasing MAPK phosphatase 1 expression and decreasing p38 phosphorylation: MAPK phosphatase 1 as a novel target for antirheumatic drugs. Arthritis Rheumatol 62:1650–1659
13. Nieminen R, Vuolteenaho K, Riutta A, Kankaanranta H, van der Kraan PM, Moilanen T, Moilanen E (2008) Aurothiomalate inhibits COX-2 expression in chondrocytes and in human cartilage possibly through its effects on COX-2 mRNA stability. Eur J Pharmacol 587:309–316
14. Sumbayev VV, Yasinska IM, Garcia CP, Gilliland D, Lall GS, Gibbs BF, Bonsall DR, Varani L, Rossi F, Calzolai L (2013) Gold nanoparticles downregulate interleukin-1beta-induced pro-inflammatory responses. Small 9:472–477
15. Tsai CY, Shiau AL, Chen SY, Chen YH, Cheng PC, Chang MY, Chen DH, Chou CH, Wang CR, Wu CL (2007) Amelioration of collagen-induced arthritis in rats by nanogold. Arthritis Rheumatol 56:544–554
16. Amin AR, Attur M, Patel RN, Thakker GD, Marshall PJ, Rediske J, Stuchin SA, Patel IR, Abramson SB (1997) Superinduction of cyclooxygenase-2 activity in human osteoarthritis-affected cartilage. Influence of nitric oxide. J Clin Invest 99:1231
17. Ghivizzani SC, Kang R, Georgescu HI, Lechman ER, Jaffurs D, Engle JM, Watkins SC, Tindal MH, Suchanek MK, McKenzie LR (1997) Constitutive intra-articular expression of human IL-1 beta following gene transfer to rabbit synovium produces all major pathologies of human rheumatoid arthritis. J Immunol 159:3604–3612
18. Notoya K, Jovanovic DV, Reboul P, Martel-Pelletier J, Mineau F, Pelletier J-P (2000) The induction of cell death in human osteoarthritis chondrocytes by nitric oxide is related to the production of prostaglandin E2 via the induction of cyclooxygenase-2. J Immunol 165:3402–3410
19. Pelletier JP, Fernandes JC, Jovanovic DV, Reboul P, Martel-Pelletier J (2001) Chondrocyte death in experimental osteoarthritis is mediated by MEK 1/2 and p38 pathways: role of cyclooxygenase-2 and inducible nitric oxide synthase. J rheumatol 28:2509–2519
20. Santangelo K, Nuovo G, Bertone A (2012) In vivo reduction or blockade of interleukin-1β in primary osteoarthritis influences expression of mediators implicated in pathogenesis. Osteoarthr Cartilage 20:1610–1618
21. Schepens SL, Kratz AL, Murphy SL (2012) Fatigability in osteoarthritis: effects of an activity bout on subsequent symptoms and activity. J Gerontol A-Biol 67(10):1114–20
22. Campos WNS, Marangoni VS, Sonego DA, Andrade MA, Colodel EM, de Souza RL (2015) Synthesis and characterization of gold nanoparticles combined with curcumin and its effect on experimental osteoarthritis in mice. Osteoarthr Cartilage 23:A397
23. Cutler C, Lattimer J, Kelsey J, Kuchuk M, OConnor D, Bal S, Katti K (2015) Nano-radiosynovectomy for osteoarthritis treatment. J NuclMed 56:363–363
24. Dwivedi P, Nayak V, Kowshik M (2015) Role of gold nanoparticles as drug delivery vehicles for chondroitin sulfate in the treatment of osteoarthritis. Biotechnol Progr 31:1416–1422
25. Vo KDN, Kowandy C, Dupont L, Coqueret X, Hien NQ (2014) Radiation synthesis of chitosan stabilized gold nanoparticles comparison between e – beam and γ irradiation. Radiat Phys Chem 94:84–87
26. Liang Q, Wang XP, Chen TS (2014) Resveratrol protects rabbit articular chondrocyte against sodium nitroprusside-induced apoptosis via scavenging ROS. Apoptosis 19:1354–1363
27. Quan YY, Qin GQ, Huang H, Liu YH, Wang XP, Chen T-S (2016) Dominant roles of Fenton reaction in sodium nitroprusside-induced chondrocyte apoptosis. Free Radical Bio and Med 94:135–144
28. Hsieh DS, Lu HC, Chen CC, Wu CJ, Yeh MK (2012) The preparation and characterization of gold-conjugated polyphenol nanoparticles as a novel delivery system. Int J Nanomed 7:1623–1633

29. Shukla R, Bansal V, Chaudhary M, Basu A, Bhonde RR, Sastry M (2005) Biocompatibility of gold nanoparticles and their endocytotic fate inside the cellular compartment: a microscopic overview. Langmuir 21:10644–10654
30. Lee H, Lee MY, Bhang SH, Kim B-S, Kim YS, Ju JH, Kim KS, Hahn SK (2014) Hyaluronate–gold nanoparticle/tocilizumab complex for the treatment of rheumatoid arthritis. ACS Nano 8:4790–4798
31. Huang YJ, Shiau AL, Chen SY, Chen YL, Wang CR, Tsai CY, Chang MY, Li YT, Leu CH, Wu CL (2012) Multivalent structure of galectin-1-nanogold complex serves as potential therapeutics for rheumatoid arthritis by enhancing receptor clustering. Eur Cells Mater 23:170–181
32. Leonavičienė L, Kirdaitė G, Bradūnaitė R, Vaitkienė D, Vasiliauskas A, Zabulytė D, Ramanavičienė A, Ramanavičius A, Ašmenavičius T, Mackiewicz Z (2012) Effect of gold nanoparticles in the treatment of established collagen arthritis in rats. Medicina (Kaunas) 48:91–101
33. Alkilany AM, Murphy CJ (2010) Toxicity and cellular uptake of gold nanoparticles: what we have learned so far? J Nanopart Res 12:2313–2333
34. Cui W, Li J, Zhang Y, Rong H, Lu W, Jiang L (2012) Effects of aggregation and the surface properties of gold nanoparticles on cytotoxicity and cell growth. Nanomed-Nanotechnol 8:46–53
35. Pan Y, Neuss S, Leifert A, Fischler M, Wen F, Simon U, Schmid G, Brandau W, Jahnen-Dechent W (2007) Size-dependent cytotoxicity of gold nanoparticles. Small 3:1941–1949
36. Pascarelli NA, Moretti E, Terzuoli G, Lamboglia A, Renieri T, Fioravanti A, Collodel G (2013) Effects of gold and silver nanoparticles in cultured human osteoarthritic chondrocytes. J Appl Toxicol 33:1506–1513
37. Hsu SH, Yen HJ, Tsai CL (2007) The response of articular chondrocytes to type II collagen-Au nanocomposites. Artif Organs 31:854–868
38. Sabella S, Brunetti V, Vecchio G, Galeone A, Maiorano G, Cingolani R, Pompa PP (2011) Toxicity of citrate-capped AuNPs: an in vitro and in vivo assessment. J Nanopart Res 13:6821–6835
39. Fu Z, Zhou X, Xing D (2013) Sensitive colorimetric detection of Listeria monocytogenes based on isothermal gene amplification and unmodified gold nanoparticles. Methods 64:260–266
40. Bastus NG, Comenge J, Puntes V (2011) Kinetically controlled seeded growth synthesis of citrate-stabilized gold nanoparticles of up to 200 nm: size focusing versus Ostwald ripening. Langmuir 27:11098–11105
41. Frens G (1973) Controlled nucleation for the regulation of the particle size in monodisperse gold suspensions. Nature 241:20–22
42. Pong B-K, Elim HI, Chong J-X, Ji W, Trout BL, Lee J-Y (2007) New insights on the nanoparticle growth mechanism in the citrate reduction of gold (III) salt: formation of the Au nanowire intermediate and its nonlinear optical properties. J Phys Chem C 111:6281–6287
43. Turkevich J, Stevenson PC, Hillier J (1951) A study of the nucleation and growth processes in the synthesis of colloidal gold. Discuss Faraday Soc 11:55–75
44. Chen T, Chen M, Chen J (2013) Ionizing radiation potentiates dihydroartemisinin-induced apoptosis of A549 cells via a caspase-8-dependent pathway. PLos One 8:e59827
45. Gao W, Xiao F, Wang X, Chen T (2013) Artemisinin induces A549 cell apoptosis dominantly via a reactive oxygen species-mediated amplification activation loop among caspase-9, −8 and −3. Apoptosis 18:1201–1213
46. Zhang W, Wang X, Chen T (2012) Resveratrol induces apoptosis via a Bak-mediated intrinsic pathway in human lung adenocarcinoma cells. Cell Signal 24:1037–1046
47. Lu YY, Chen TS, Wang XP, Li L (2010) Single-cell analysis of dihydroartemisinin–induced apoptosis through reactive oxygen species–mediated caspase-8 activation and mitochondrial pathway in ASTC-a-1 cells using fluorescence imaging techniques. J biomed Opt 15(4):046028
48. Takikawa Y, Miyoshi H, Rust C, Roberts P, Siegel R, Mandal PK, Millikan RE, Gores GJ (2001) The bile acid–activated phosphatidylinositol 3-kinase pathway inhibits Fas apoptosis upstream of bid in rodent hepatocytes. Gastroenterology 120:1810–1817
49. Brown CL, Whitehouse MW, Tiekink ER, Bushell GR (2008) Colloidal metallic gold is not bio-inert. Inflammopharmacology 16:133–137
50. Chen YS, Hung YC, Liau I, Huang GS (2009) Assessment of the in vivo toxicity of gold nanoparticles. Nanoscale Res Lett 4:858–864
51. Zhang XD, Wu D, Shen X, Liu PX, Yang N, Zhao B, Zhang H, Sun YM, Zhang LA, Fan FY (2011) Size-dependent in vivo toxicity of PEG-coated gold nanoparticles. Int J Nanomed 6:2071–2081
52. Villiers C, Freitas H, Couderc R, Villiers MB, Marche P (2010) Analysis of the toxicity of gold nano particles on the immune system: effect on dendritic cell functions. J Nanopart Res 12:55–60
53. Patra HK, Banerjee S, Chaudhuri U, Lahiri P, Dasgupta AK (2007) Cell selective response to gold nanoparticles. Nanomed-Nanotechnol 3:111–119
54. Pan Y, Leifert A, Ruau D, Neuss S, Bornemann J, Schmid G, Brandau W, Simon U, Jahnen-Dechent W (2009) Gold nanoparticles of diameter 1.4 nm trigger necrosis by oxidative stress and mitochondrial damage. Small 5: 2067–2076
55. Mkandawire MM, Lakatos M, Springer A, Clemens A, Appelhans D, Krause-Buchholz U, Pompe W, Rödel G, Mkandawire M (2015) Induction of apoptosis in human cancer cells by targeting mitochondria with gold nanoparticles. Nanoscale 7:10634–10640
56. Buckwalter J, Mankin H (1997) Articular cartilage: tissue design and chondrocyte-matrix interactions. Instr course lect 47:477–486
57. Tay CY, Yu Y, Setyawati MI, Xie J, Leong DT (2014) Presentation matters: identity of gold nanocluster capping agent governs intracellular uptake and cell metabolism. Nano Res 7:805–815
58. Chompoosor A, Saha K, Ghosh PS, Macarthy DJ, Miranda OR, Zhu ZJ, Arcaro KF, Rotello VM (2010) The role of surface functionality on acute cytotoxicity, ROS generation and DNA damage by cationic gold nanoparticles. Small 6:2246–2249
59. Deshiikan S, Papadopoulos K (1998) Modified Booth equation for the calculation of zeta potential. Colloid Polymer Sci 276:117–124
60. Vorwerg L, Antonietti M, Tauer K (1999) Electrophoretic mobility of latex particles: effect of particle size and surface structure. Colloids Surfaces A 150:129–135